PNAS RESEARCH ARTICLE | CHEMISTRY

Resolving the amine-promoted hydrolysis mechanism of N_2O_5 under tropospheric conditions

Chuan Zhou[a,1], Bai Li[a,1], Jingyan Zhang[a], Graeme Henkelman[b,c], Joseph S. Francisco[d,2], and Lei Li[a,2]

Contributed by Joseph S. Francisco; received April 1, 2022; accepted August 24, 2022; reviewed by Anastassia Alexandrova and De-en Jiang

Hydrolysis of N_2O_5 under tropospheric conditions plays a critical role in assessing the fate of O_3, OH, and NO_x in the atmosphere. However, its removal mechanism has not been fully understood, and little is known about the role of entropy. Herein, we propose a removal path of N_2O_5 on the water clusters/droplet with the existence of amine, which entails a low free-energy barrier of 4.46 and 3.76 kcal/mol on a water trimer and droplet, respectively, at room temperature. The free-energy barrier exhibits strong temperature dependence; a barrierless hydrolysis process of N_2O_5 at low temperature (≤150 K) is observed. By coupling constrained ab initio molecular dynamics (constrained AIMD) simulations with thermodynamic integration methods, we quantitively evaluated the entropic contributions to the free energy and compared NH_3-, methylamine (MA)-, and dimethylamine (DMA)-promoted hydrolysis of N_2O_5 on water clusters and droplet. Our results demonstrate that methylation of NH_3 stabilizes the product state and promotes hydrolysis of N_2O_5 by reducing the free-energy barriers. Furthermore, a quantitative analysis of the internal coordinate distribution of the reaction center and the relative position of surrounding species reveals that the significant entropic contribution primarily results from the ensemble effect of configurations observed in the AIMD simulations. Such an ensemble effect becomes more significant with more water molecules included. Lowering the temperature effectively minimizes the entropic contribution, making the hydrolysis more exothermic and barrierless. This study sheds light on the importance of the promoting effect of amines and the entropic effect on gas-phase hydrolysis reactions, which may have far-reaching implications in atmospheric chemistry.

N_2O_5 | amines | entropy | hydrolysis | anharmonic effect

The N_2O_5 molecule, as a key reservoir species for nitrogen oxide in the atmosphere, plays a vital role in regulating the atmospheric level of NO_x and dominates the cycle of the primary tropospheric oxidants, including HO_x radicals and ozone. The nocturnal removal of N_2O_5 is essential to the establishment of the oxidation reaction network in the atmosphere and has attracted significant attention in determining the air quality (1–3). In experiments, the uptake of N_2O_5 and its dependence on the atmospheric environment are widely investigated with field measurements and parameterized kinetic models (4–10). However, no detailed atomic-level mechanism is provided from these measurements, which largely hinders rationalization of experimental observations (11–14). Theoretically, various removal mechanisms have been proposed on the basis of computational simulations. Still, predicted rate constants are much smaller than the experimental value by 2 to 10 orders of magnitude, mainly due to the involvement of high energy barriers (>14 kcal/mol) (11, 15–19). The discrepancies between theory and experiment suggest that one or more removal mechanisms of N_2O_5 have yet to be identified.

Various routes have been reported for the uptake of N_2O_5, including direct dry decomposition (12–14), homogeneous hydrolysis (9, 20), halogen activation (21–23), and heterogeneous uptake by solids (such as NaCl) (24), aerosols and solutions (such as H_2SO_4, $(NH_4)_2SO_4$, etc.) (25, 26). Among these routes, the hydrolysis of N_2O_5 to HNO_3 is believed to be responsible for 25 to 41% of the removal of tropospheric N_2O_5 (5, 27–29). The hydrolysis of N_2O_5 with a single water molecule has been reported with an energy barrier of 21.1 kcal/mol. Additional water molecules (up to trimers) can significantly reduce the energy barrier and promote the hydrolysis of nitrogen oxides due to the solvent effect (11, 16). As reported by Liedl and coworkers (11), the hydrolysis barrier decreases to 14.2 kcal/mol in the presence of three water molecules. The rate constants calculated from these reaction mechanisms are much smaller than those from laboratory studies (11). Galib and Limmer (30) proposed an alternative interfacial reactive uptake model on atmospheric aerosol. They found that the direct hydrolysis of N_2O_5 has a relatively low free-energy barrier of 3.8 kcal/mol and

Significance

The hydrolysis of N_2O_5, as a primary source of nitrate, has attracted significant attention in determining the fate of many gaseous species in the atmosphere. Despite its importance, its removal mechanism remains far from understood. Based on constrained ab initio molecular dynamics simulations and thermodynamic integration methods, a comparison of NH_3-, MA-, and DMA-assisted hydrolysis of N_2O_5 on the water clusters/droplet sheds light on the promoting role of the methylation of NH_3. More importantly, a quantitative analysis of the entropic contribution to the reaction is achieved by considering the ensemble effect of configurations. This finding provides insight into the hydrolysis reaction, which is essential to the nucleation of aerosol particles in atmospheric chemistry.

Author contributions: G.H., J.S.F., and L.L. designed research; C.Z., B.L., J.Z., and L.L. performed research; J.S.F. analyzed data; and C.Z., B.L., G.H., J.S.F., and L.L. wrote the paper.

Reviewers: A.A., University of California, Los Angeles; and D.J., University of California, Riverside.

The authors declare no competing interest.

[1]C.Z. and B.L. contributed equally to this work.

[2]To whom correspondence may be addressed. Email: frjoseph@sas.upenn.edu or lil33@sustech.edu.cn.

This article contains supporting information online at http://www.pnas.org/lookup/suppl/doi:10.1073/pnas.2205668119/-/DCSupplemental.

Published September 19, 2022.

claimed that the uptake and hydrolysis process of N_2O_5 is dominated by interfacial processes rather than in bulk, which emphasizes the importance of the air–water interface for atmospheric reactions.

Gaseous alkaline molecules have been reported to have a strong catalytic effect on the hydrolysis of atmospheric molecules and enhance the nucleation of aerosol particles. For example, NH_3, as a primary alkaline gaseous species in the atmosphere, significantly promotes the formation of HONO (31, 32) and the heterogeneous reaction of SO_2 to sulfate (33) under atmospheric conditions. Methylamine (MA) and dimethylamine (DMA), as the most common organic bases, also exhibit promoting effects on atmospheric reactions, such as the hydrolysis of SO_2 (34), formation of nitrated phenolic compounds (35), etc. Kirkby and coworkers (36) showed that DMA accelerates particle formation by 1,000-fold compared with NH_3 due to a solid acid–amine stabilization effect. Wang and coworkers (37) also reported the correlation of a high particle formation rate with a high concentration of H_2SO_4–DMA–H_2O nuclei. Despite these achievements, little work has been conducted on the hydrolysis of N_2O_5 with the existence of amines. Resolving the potential promotion effect of amines on the hydrolysis of N_2O_5 is highly desired and essential to rationalize experimental observations and understand the nucleation of aerosol particles in the atmosphere.

This work systematically studies NH_3-, MA-, and DMA-promoted hydrolysis of N_2O_5 on the water monomer, dimer, trimer, and droplet by coupling ab initio molecular dynamics (AIMD) simulations and the thermodynamics integration (TI) method. Our results demonstrate the promoting effect of the amines on the hydrolysis of N_2O_5. A low free-energy barrier of 4.46 kcal/mol is characterized for the DMA-promoted hydrolysis of N_2O_5 in the water trimer system. More importantly, we coupled the TI method with the constrained AIMD method to explicitly evaluate entropic contributions (including anharmonic effects) on the hydrolysis reaction. The entropic contribution is critical to atmospheric reactions but difficult to treat accurately in computational simulations. Statistical thermodynamic methods based upon the harmonic approximation (denoted as the HA method) are widely used to compute the entropic contribution of atmospheric reactions. However, the HA method fails to provide a reliable assessment of entropy toward more-complex systems or reactions at evaluated temperatures where large-amplitude collective motion of water molecules and ensemble effect dominate the free-energy landscape. Here, we show that the entropic effect plays a dominant role in the amine-promoted hydrolysis of N_2O_5 and quantitively analyze the origin of entropic contribution, providing a model method for future investigation of the entropic effect on atmospheric reactions.

Results and Discussion

NH_3-, MA-, and DMA-Promoted Hydrolysis of N_2O_5. To understand the amine effect, we systematically studied the hydrolysis of N_2O_5 on the water monomer, dimer, and trimer in the presence of NH_3, MA, and DMA. A significant promoting effect of methylation of NH_3 is observed in all systems. Here, we take the water trimer system as an example. Although it is about one order of magnitude less abundant than the water dimer, it is still crucial for hydrolysis reactions in the atmosphere (38, 39). Following Eq. **1**, we first computed energy profiles for hydrolysis of N_2O_5 with NH_3, MA, and DMA on the water trimer with the climbing image nudged elastic band (CI-NEB) method (Fig. 1 *A* and *B*),

$$N_2O_5 + 3H_2O + X \rightarrow HNO_3 + NO_3^- + HX^+ + 2H_2O, \quad [1]$$

where X represents NH_3, MA, or DMA.

As shown in Fig. 1*A*, the hydrolysis of N_2O_5 in all three systems follows a concerted single-water mechanism with only one water molecule directly involved in the reaction, as reported previously (11). Metadynamics simulations (*SI Appendix*, Fig. S1) further confirm the concerted mechanism. In such a mechanism, one water molecule is sandwiched between the N_2O_5 and X species, forming a reaction center. The two remaining water molecules form a dimer which interacts with the reaction center through hydrogen bonds. During the reaction, N_2O_5 approaches the OH group of the water, generating a HNO_3 molecule and a NO_3^- group. The remaining H^+ interacts with X to produce HX^+. Following the single-water mechanism, the hydrolysis of N_2O_5 in the NH_3 system requires overcoming an energy barrier of ~7.93 kcal/mol. With the presence of MA, a lower barrier of ~3.95 kcal/mol is found, suggesting a promoting effect from the methylation of NH_3. The further methylation of NH_3 (corresponding to the DMA system) leads to a barrierless hydrolysis process. The reaction becomes exothermic with an enthalpy change of −24.26 kcal/mol. The huge enthalpy change in the DMA system results from the stronger Coulomb interaction of the $HDMA^+$–NO_3^- ion pair, as shown by the Mulliken population analysis (*SI Appendix*, Fig. S3). Overall, the energy profiles computed with the CI-NEB method confirm the promoting role of the methylation of NH_3 toward the hydrolysis of N_2O_5, similar to that observed in the hydrolysis of SO_2 (34).

Entropic contributions are not considered in the energy profiles discussed above, but they could be potentially critical to the gas-phase reaction. Accordingly, we computed the free-energy change (ΔG) along the selected collective variable (CV) for these systems at 300 K using the TI method. The sum of N_3–H_1 and N_2–O_3 distance is chosen as the CV. The free-energy profiles are presented in Fig. 1*C*, and the reaction coordinates are normalized with the following equation:

$$R_{\text{normalized}} = \frac{R_{\max} - R_i}{R_{\max} - R_{\min}}, \quad [2]$$

where $R_{\max}$, $R_{\min}$, and R_i are the maximum, minimum, and instantaneous CV values, respectively. The computed free-energy barriers for the NH_3, MA, and DMA systems are 10.40, 7.73, and 4.46 kcal/mol, respectively, following the same order as energy barriers computed with the CI-NEB method. The hydrolysis of N_2O_5 in the DMA system has the most negative free-energy change (−22.49 kcal/mol), compared with the NH_3 and MA systems. These results demonstrate that the methylation of NH_3 favors the hydrolysis of N_2O_5.

Unlike the energy profiles shown in Fig. 1*B*, a relatively high barrier is observed from the free-energy calculations for each system. Such a phenomenon is most typical in the DMA system. Based on the CI-NEB method, the DMA-assisted hydrolysis of N_2O_5 is barrierless, but a free-energy barrier of 4.46 kcal/mol is found when entropy is considered. The free-energy barriers for the NH_3 and MA system are 2.47 and 3.78 kcal/mol higher than the energy barrier computed with the CI-NEB method. These results suggest a significant entropic effect on the hydrolysis of N_2O_5. The computed reaction rates are 1.2×10^{24}, $3.5 \times 10^{24\sim25}$, and $7.4 \times 10^{24\sim25}$ molecules per cm^3/s^1 for the NH_3-, MA-, and DMA-promoted hydrolysis, respectively, of N_2O_5 on the water trimer (*SI Appendix*, Table S1). The same trend is observed for the monomer system (*SI Appendix*, Table S1). Although the concentrations are two to three orders of

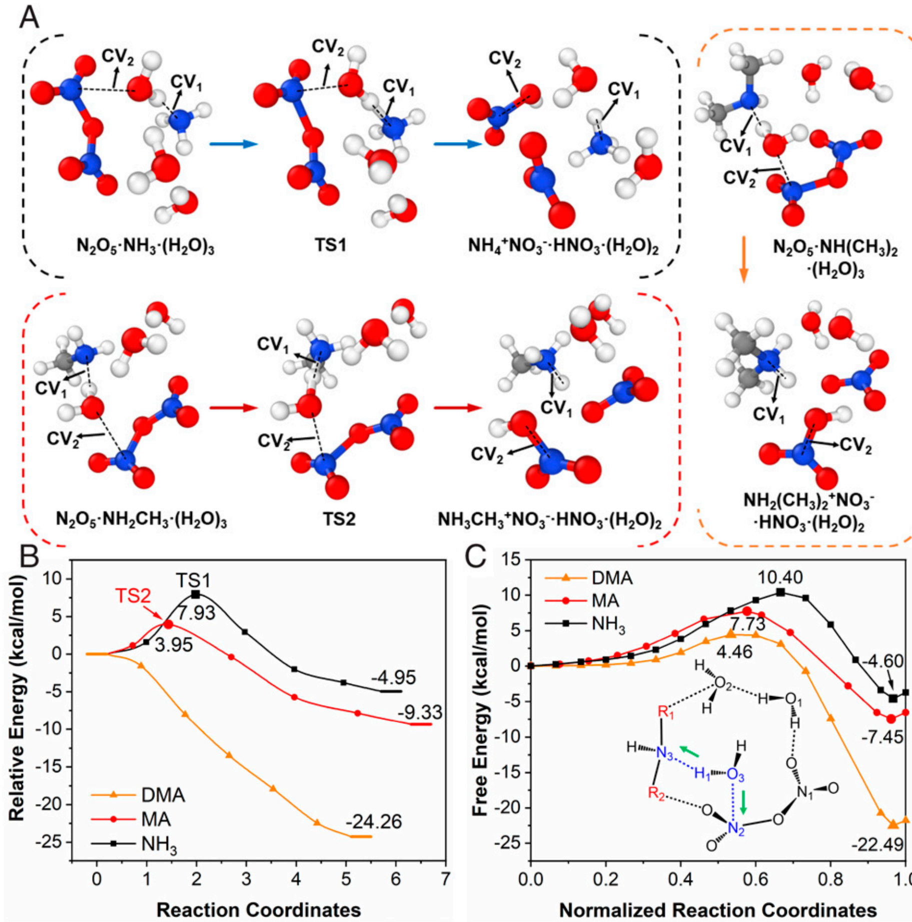

Fig. 1. (*A*) Atomic structures of the initial, final, and transition states (TS) for the hydrolysis of N_2O_5 with the existence of NH_3, MA, and DMA on the water trimer. The white, blue, and red balls represent H, N, and O atoms, respectively. (*B*) Energy profiles for the hydrolysis of N_2O_5 in the presence of NH_3, MA, and DMA on the water trimer based on the CI-NEB method. (*C*) Free-energy profiles for the hydrolysis of N_2O_5 with the presence of NH_3, MA, and DMA on the water trimer at 300 K using the TI method. *Inset* illustrates their initial structures, where the red R_1 and R_2 represent $-CH_3$ or $-H$ groups. The CV along the free-energy coordinate is set as the sum of the $N_3–H_1$ and $N_2–O_3$ distances. Green arrows indicate the direction of the corresponding atom's motion along the reaction coordinate.

magnitude lower than the NH_3, the MA- and DMA-promoted N_2O_5 hydrolysis processes are 3 to ∼30 and 6 to ∼60 times faster, respectively, than the NH_3 system (*SI Appendix*), confirming the promoting role of the MA and DMA.

Temperature Dependence. To confirm the entropic effect, we computed free-energy profiles of the hydrolysis of N_2O_5 in all three systems at four different temperatures (50, 150, 250, and 300 K) using the TI method. The computed free-energy profiles are presented in Fig. 2*A* for the DMA system and in *SI Appendix*, Fig. S4 for the NH_3 and MA systems. The change in the free-energy barriers with temperature is shown in Fig. 2*B* for all three systems.

As shown in Fig. 2, both the free-energy barrier and the reaction free-energy change exhibit temperature dependence. At 300 K, the hydrolysis of N_2O_5 with the existence of DMA entails a free-energy barrier of 4.46 kcal/mol. This barrier decreases to 3.12 kcal/mol at 250 K and vanishes at 50 and 150 K, leading to a barrierless hydrolysis process. Similarly, the free-energy change of the reaction becomes more negative with decreasing temperature. The same trend is observed for the NH_3 and MA systems (*SI Appendix*, Fig. S4 and Fig. 2*B*). As shown in Fig. 2*B*, the free-energy barriers for NH_3 and MA systems increase linearly with temperature. That indicates that low temperature favors the hydrolysis of N_2O_5 for all three systems, confirming a significant entropic effect on the hydrolysis of N_2O_5.

Entropic Effect. To understand the origin of the entropic effects, we evaluated the free energy from the partition functions, as described in ref. 40. In this method, the entropy is calculated as the sum of contributions from translational (S_{trans}), rotational (S_{rot}), and vibrational (S_{vib}) motion with the HA method. For comparison, the variation of the ΔG of the hydrolysis of N_2O_5 obtained from the HA (in black) and TI (in red) methods is presented in Fig. 3*A*. Clearly, ΔG computed from these two methods exhibits very different temperature dependence. For the HA method, little change of ΔG is observed with increasing temperature. A detailed analysis of the entropic contribution from each component indicates that the difference of entropy between the reactant and product state at each temperature is negligible (*SI Appendix*, Fig. S5), leading to little entropy variation with temperature. In contrast, ΔG calculated with the TI method increases significantly with temperature, showing that entropy decreases upon the hydrolysis of N_2O_5 ($\Delta S < 0$). The same results are observed for the NH_3 and MA systems (*SI Appendix*, Fig. S5).

The inconsistency between the HA and TI methods arises from anharmonicities in each vibrational mode and the contributions of multiple potential wells. We evaluated the anharmonicities of the selected reaction path in Fig. 1*A* for the DMA

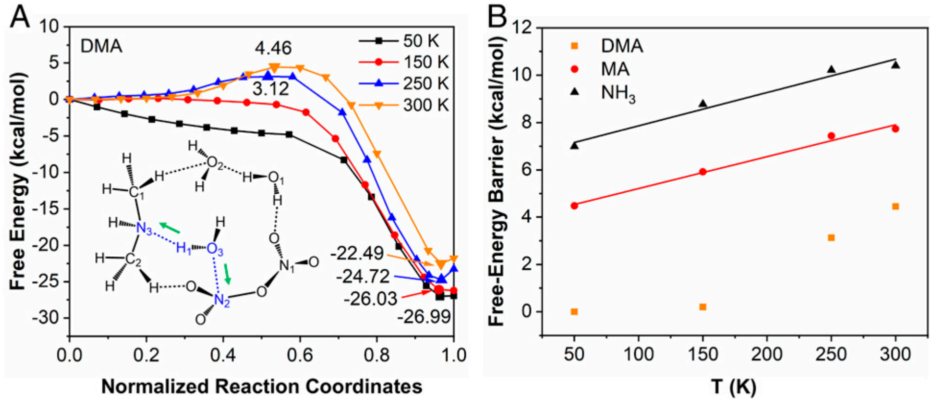

Fig. 2. (*A*) Free energy profiles and (*B*) variation of free-energy barriers with temperature for the DMA-assisted hydrolysis of N_2O_5 on the water trimer at 50, 150, 250, and 300 K computed with the TI method. *Inset* in *A* illustrates the initial structure, and the CV is set as the sum of the N_3–H_1 and N_2–O_3 distances.

trimer system by computing the anharmonic vibrational frequencies (*SI Appendix*, Fig. S6). The linear dependence of $-T\Delta S$ on temperature confirms anharmonic contributions. By extracting and optimizing snapshot structures from MD simulations, we observed the existence of various isomers, suggesting the presence of multiple potential wells (*SI Appendix*, Fig. S7). It is hard to quantitatively evaluate the contributions of each part individually. Instead, we computed the overall entropic contribution by counting the probability of each configuration observed in the MD simulations and treated all configurations as an ensemble.

Upon checking trajectories of the MD simulations, we noticed that the entropic contribution to the free energy results from two parts, the reaction center and surrounding species (Fig. 3*B*). The reaction center consists of a tetrahedron formed by atoms H_1, N_3, N_2, and O_3, which can be defined by four angles ($\theta_{H_1N_3O_3}$, $\theta_{H_1O_3N_3}$, $\theta_{N_2N_3O_3}$, and $\theta_{N_3O_3N_2}$) and a dihedral angle θ_{H_1} formed by plane N_3–O_3–N_2 and plane N_3–O_3–H_1. Water molecules, the $-CH_3$ and $-NO_3$ groups around the reaction center, are identified as surrounding species (denoted as *Y*). To evaluate their contributions, we defined a dihedral angle (θ_Y) between the plane of N_3–O_3–N_2 (in the reaction center) and N_3–O_3–Y to describe the relative position of the target surrounding species.

Taking surrounding species as an example, Fig. 4 shows the distribution of θ_Y ($g(\theta_Y)$) with $Y = O_1$, which describes the motion of the H_2O with O_1 as the center atom (denoted as $(H_2O)^1$) in the reactant and product state at 50, 150, and 300 K. The distribution of other target atoms in different systems is shown in *SI Appendix*, Figs. S8–S10, and exhibits similar behavior. As an example, at 50 K, θ_{O_1} exhibits a sharp distribution in the reactant and product states, indicating a narrow region of motion of $(H_2O)^1$. At higher temperatures (150 and 300 K), the distribution of θ_{O_1} spreads over a much wider range, that is, from $-180°$ to $180°$ in the reactant state, indicating that higher temperature activates modes that are inactive at a lower temperature. At a specific temperature, θ_{O_1} in the product state generally has a narrower distribution than that in the reactant state, implying a decrease of entropy during the hydrolysis of N_2O_5, which is consistent with the observed positive correlation of ΔG with temperature, as shown in Fig. 3*A*.

Based on the $g(\theta)$, the entropy change contribution ($T\Delta S$) to the free energy is computed by quantitively evaluating the entropy of reactant and product states. The entropy for each state is calculated with the following equation, as established by Boltzmann and Gibbs:

$$S = \sum_{RC} S_{RC} + \sum_{SS} S_{SS} = -k_B \sum_{RC}\sum_{i} p_i \ln p_i - k_B \sum_{SS}\sum_{j} p_j \ln p_j, \qquad [3]$$

where S_{RC} and S_{SS} represent the entropic contribution from the reaction center and surrounding species *SS* ($SS = H_2O$, $-CH_3$, or $-NO_3$), respectively; p_i (p_j) is the probability of the microstate i (j) labeled with the defined angle or dihedral angle of internal coordinates, corresponding to the point at the curve of distribution functions (*SI Appendix*, Figs. S8–S10). The variation of the computed $-T\Delta S$ with temperature is shown in

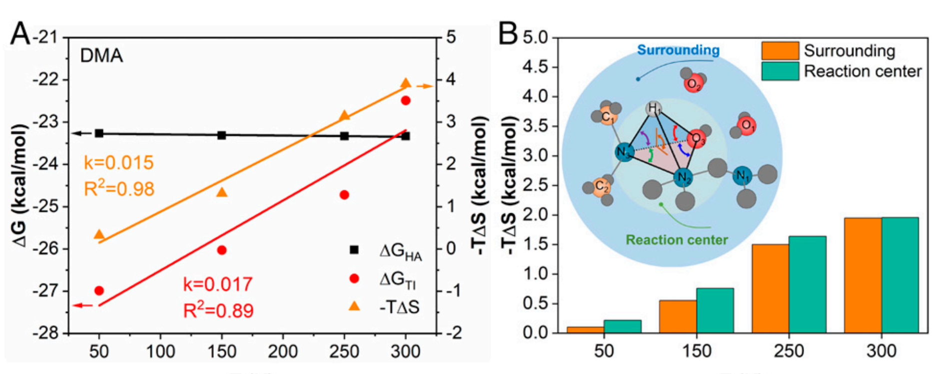

Fig. 3. (*A*) Scaling relations between ΔG and temperature for the DMA-assisted hydrolysis of N_2O_5 on the water trimer. ΔG_{HA} *and* ΔG_{TI} represent the free-energy change calculated with the HA and TI methods. $-T\Delta S$ is the entropic contribution to the free-energy obtained from the TI method. Note that k is the slope of the scaling relation. (*B*) Entropic contributions of the reaction center and the surrounding species (defined in the *Inset*) for the DMA-promoted hydrolysis of N_2O_5 on the water trimer. The small and large grey spheres in the *Inset* represent H and O atoms, respectively.

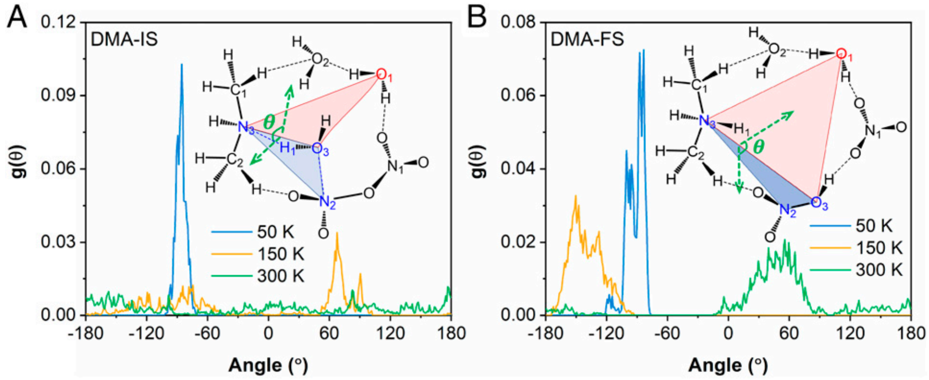

Fig. 4. Dihedral angle distribution function $g(\theta)$ of (*A*) initial state and (*B*) final state for the O_1 in the DMA-assisted hydrolysis process of N_2O_5 at 50, 150, and 300 K. The dihedral angle is defined as the angle between the N_3–O_3–O_1 and N_3–O_3–N_2 planes as noted in *Insets*.

Fig. 3*A* for the DMA system and in *SI Appendix*, Fig. S5 for the NH_3 and MA systems. As shown in Fig. 3*A*, $-T\Delta S$ for the hydrolysis of N_2O_5 in the DMA system increases linearly with temperature, as observed in the variation of the free-energy change from the TI method. Moreover, the linear dependence of $-T\Delta S$ with temperature entails a slope close to that of the free-energy change. A detailed analysis suggests that the entropic contributions from both surrounding species and the reaction center increase with temperature (Fig. 3*B*). Notably, the surrounding species' contribution becomes increasingly important with the temperature increase. Similar results are found for the NH_3 and MA systems (*SI Appendix*, Fig. S11). The good agreement between the temperature dependence of $-T\Delta S$ and the free-energy change demonstrates that the ensemble effect of configurations is responsible for the entropic contribution to the hydrolysis of N_2O_5. Each configuration can be identified with the internal coordinates of the reaction center and positions of surrounding species relative to the reaction center. As such, the ensemble effect of configurations can be quantitatively evaluated with the distribution of as-defined internal coordinates.

The Amine-Promoted Hydrolysis of N_2O_5 on Water Clusters/Droplet. We have demonstrated the importance of entropy and the promoting role of the MA and DMA in the water trimer system compared to NH_3. Here, we further examine the hydration effect on the hydrolysis of N_2O_5 by computing the free-energy profiles of the reaction on the water monomer, dimer, and droplet (Fig. 5) at 300 K for the MA and DMA systems with the TI method. The hydrolysis of N_2O_5 in the monomer, dimer, and droplet systems follows the same single-water mechanism as that observed in the trimer system (*SI Appendix*, Figs. S12–S14). The free-energy profiles in Fig. 5 show that the free-energy barriers for both the MA and DMA systems decrease with extra water molecules included. The decrease in the energy barrier is insignificant, consistent with previous reports that water in atmospheric aerosols has a small effect on the N_2O_5 uptake (4). Specifically, the free-energy barriers of the MA-promoted hydrolysis reaction are 8.37, 7.92, 7.73, and 6.13 kcal/mol for the water monomer, dimer, trimer, and droplet systems, respectively. In contrast, lower free-energy barriers are involved in the DMA-promoted hydrolysis process with values of 6.67, 6.12, 4.46, and 3.76 kcal/mol for the water monomer, dimer, trimer, and droplet systems, respectively, confirming the promoting role of the methylation extent. The entropic contribution from the ensemble effect of configurations becomes more pronounced with the number of water molecules increasing (Fig. 5, *Insets*). Notably, the DMA-promoted hydrolysis of N_2O_5 on the water droplet entails the lowest free-energy barrier, with a value of 3.76 kcal/mol at 300 K, shedding light on the importance of clouds in the atmosphere.

Conclusions

In summary, we performed constrained AIMD simulations directed by the TI method to systematically investigate the hydrolysis of N_2O_5 on the water monomer, dimer, trimer, and water droplet with the existence of NH_3, MA, and DMA. We found that the methylation of NH_3 largely promotes the hydrolysis of N_2O_5. Remarkably, DMA facilitates a low free-energy barrier hydrolysis process with values of 4.46 and 3.76 kcal/mol

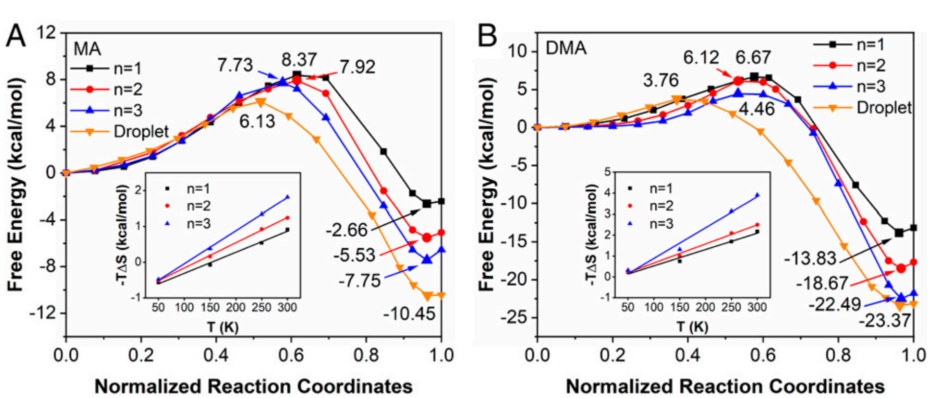

Fig. 5. Free-energy profiles for the (*A*) MA- and (*B*) DMA-assisted hydrolysis of N_2O_5 on the water monomer, dimer, trimer, and droplet; "*n*" represents the number of water molecules in the system. *Insets* show the scaling relations between $-T\Delta S$ and temperature for the monomer, dimer, and trimer systems.

at room temperature for the trimer and droplet systems, respectively. A significant entropic effect is observed and suppresses the reaction at higher temperatures; remarkably, the DMA-promoted hydrolysis of N_2O_5 becomes a barrierless process at temperatures below 150 K. Furthermore, the role of entropy at the configurational ensemble level is understood by considering the distribution of internal coordinates of the reaction center and relative positions of surrounding species. Finally, we identified the role of additional water molecules in promoting the hydrolysis of N_2O_5. Overall, these findings deepen our understanding of the role of entropic effects and propose a path for the removal of tropospheric N_2O_5 on the water clusters/droplet in the presence of amine, which could facilitate the rational identification of nucleation of aerosol particles in atmospheric chemistry.

Methods

The constrained AIMD and CI-NEB simulations were performed using the Gaussian and plane-wave method implemented in the CP2K Quickstep package (41). The Goedecker–Teter–Hutter (42, 43) norm-conserved pseudopotentials and the wave functions expanded in a triple-ζ Gaussian basis set with additional auxiliary basis sets were adopted to model the core and valence electrons, respectively. The energy cutoffs for the finest grid level and Gaussian waves were 300 and 40 Ry, respectively. The Grimme dispersion correction method (44, 45) was used to model dispersion interactions. The Becke–Lee–Yang–Parr (BLYP) (46, 47) functional was employed to describe electronic exchange and correlation. For comparison, the B3LYP functional (48) was also used to compute the free-energy pathway for the hydrolysis of N_2O_5 (*SI Appendix*, Fig. S15). Results based on the BLYP functional exhibit the same trend as that observed for the B3LYP method.

To minimize the interaction between two neighboring clusters, a large supercell ($20 \times 20 \times 20$ Å^3) was adopted for the DMA/MA/NH_3 + N_2O_5 + nH_2O systems (n = 1, 2, and 3). A (20×20 Å^2) water slab with a thickness of ∼15 Å is chosen to simulate the hydrolysis of N_2O_5 on the water droplet containing 200 water molecules. The slab model was stabilized with classical force field methods for 100 ps and then followed by a 20-ps AIMD simulation at 300 K. The radial distribution function of the water droplet was computed (*SI Appendix*, Fig. S16) and was consistent with the previous air–water interface study (49). A CV was defined as the sum of N_3–H_1 (CV_1) and N_2–O_3 lengths (CV_2) (as labeled in Fig. 1*C*). The Gibbs free energy was computed by integrating the free-energy gradient over a series of constrained CV values with an interval of 0.2 Å along the reaction path. In the constrained AIMD simulations, the temperature was controlled at 50, 150, 250, and 300 K using the Nosé–Hoover chain method (50, 51) with the constant-volume and constant-temperature ensemble. The time step was set as 0.5 and 1 fs for the cluster and droplet models, respectively. The reactant and product state structures for each system were first equilibrated for 20 ps and used to interpolate intermediate states. Each constrained AIMD simulation was equilibrated for 2 ps to quench the average Lagrange force, and structures were then sampled for at least 20 ps to guarantee the convergence of the free-energy path (*SI Appendix*, Fig. S17). The CI-NEB (52) method implemented in the transition state library for the Atomic Simulation Environment (TSASE) was used to locate transition states (TSs). The force convergence on each image was set as 0.02 eV/Å. The vibrational frequencies were also calculated, and only one imaginary frequency was confirmed for TS. The translational, rotational, and vibrational entropies were calculated within the ideal gas limit as implemented in the Atomic Simulation Environment code (53).

Data, Materials, and Software Availability. All study data are included in the article and/or *SI Appendix*.

ACKNOWLEDGMENTS. This work is supported by the National Natural Science Foundation of China (Grant 22179058), Shenzhen fundamental research funding (Grant JCYJ20210324115809026), and Shenzhen Key Laboratory of Micro/Nano-Porous Functional Materials (Grant ZDSYS20210709112802010). Computational resources were provided by the Center for Computational Science and Engineering of the Southern University of Science and Technology and the Texas Advanced Computing Center. G.H. acknowledges the ongoing support from the Welch Foundation (Grant F-1841).

Author affiliations: [a]Shenzhen Key Laboratory of Micro/Nano-Porous Functional Materials, Department of Materials Science and Engineering, Southern University of Science and Technology, Shenzhen 518055, China; [b]Department of Chemistry, The University of Texas at Austin, Austin, TX 78712; [c]Institute for Computational Engineering and Sciences, The University of Texas at Austin, Austin, TX 78712; and [d]Department of Earth and Environmental Sciences, University of Pennsylvania, Philadelphia, PA 19104

1. J. H. Steinfeld, S. N. Pandis, *Atmospheric Chemistry and Physics: From Air Pollution to Climate Change* (Wiley, New York, 1998).
2. M. Hallquist, D. J. Stewart, J. Baker, R. A. Cox, Hydrolysis of N_2O_5 on submicron sulfuric acid aerosols. *J. Phys. Chem. A* **104**, 3984–3990 (2000).
3. J. Kleffmann, T. Gavriloaiei, Y. Elshorbany, M. Ródenas, P. Wiesen, Detection of nitric acid (HNO_3) in the atmosphere using the LOPAP technique. *J. Atmos. Chem.* **58**, 131–149 (2007).
4. M. Xia *et al.*, Heterogeneous uptake of N_2O_5 in sand dust and urban aerosols observed during the dry season in Beijing. *Atmosphere* **10**, 204 (2019).
5. E. E. McDuffie *et al.*, Heterogeneous N_2O_5 uptake during winter: Aircraft measurements during the 2015 WINTER campaign and critical evaluation of current parameterizations. *J. Geophys. Res. Atmos.* **123**, 4345–4372 (2018).
6. W. L. Chang *et al.*, Evaluating N_2O_5 heterogeneous hydrolysis parameterizations for CalNex 2010. *J. Geophys. Res. Atmos.* **121**, 5051–5070 (2016).
7. X. Wang *et al.*, Observations of N_2O_5 and $ClNO_2$ at a polluted urban surface site in North China: High N_2O_5 uptake coefficients and low $ClNO_2$ product yields. *Atmos. Environ.* **156**, 125–134 (2017).
8. J. Hjorth, G. Ottobrini, F. Cappellani, G. Restelli, Fourier transform infrared study of the rate constant of the homogeneous gas-phase reaction N_2O_5+H_2O and determination of absolute infrared band intensities of N_2O_5 and HNO_3. *J. Phys. Chem.* **91**, 1565–1568 (1987).
9. T. F. Mentel, D. Bleilebens, A. Wahner, A study of nighttime nitrogen oxide oxidation in a large reaction chamber—The fate of NO_2, N_2O_5, HNO_3, and O_3 at different humidities. *Atmos. Environ.* **30**, 4007–4020 (1996).
10. A. Wahner, T. F. Mentel, M. Sohn, Gas-phase reaction of N_2O_5 with water vapor: Importance of heterogeneous hydrolysis of N_2O_5 and surface desorption of HNO_3 in a large Teflon chamber. *Geophys. Res. Lett.* **25**, 2169–2172 (1998).
11. A. F. Voegele, C. S. Tautermann, T. Loerting, K. R. Liedl, Toward elimination of discrepancies between theory and experiment: The gas-phase reaction of N_2O_5 with H_2O. *Phys. Chem. Chem. Phys.* **5**, 487–495 (2003).
12. M. Mozurkewich, J. G. Calvert, Reaction probability of N_2O_5 on aqueous aerosols. *J. Geophys. Res.* **93**, 15889–15896 (1988).
13. A. G. Russell, G. R. Cass, J. H. Seinfeld, On some aspects of nighttime atmospheric chemistry. *Environ. Sci. Technol.* **20**, 1167–1172 (1986).
14. B. Alexander *et al.*, Global inorganic nitrate production mechanisms: Comparison of a global model with nitrate isotope observations. *Atmos. Chem. Phys.* **20**, 3859–3877 (2020).
15. D. Hanway, F.-M. Tao, A density functional theory and ab initio study of the hydrolysis of dinitrogen pentoxide. *Chem. Phys. Lett.* **285**, 459–466 (1998).
16. J. A. Snyder, D. Hanway, J. Mendez, A. J. Jamka, F.-M. Tao, A density functional theory study of the gas-phase hydrolysis of dinitrogen pentoxide. *J. Phys. Chem. A* **103**, 9355–9358 (1999).
17. J. P. McNamara, I. H. Hillier, Exploration of the atmospheric reactivity of N_2O_5 and HCl in small water clusters using electronic structure methods. *Phys. Chem. Chem. Phys.* **2**, 2503–2509 (2000).
18. J. P. McNamara, I. H. Hillier, Structure and reactivity of dinitrogen pentoxide in small water clusters studied by electronic structure calculations. *J. Phys. Chem. A* **104**, 5307–5319 (2000).
19. I. M. Alecu, P. Marshall, Computational study of the thermochemistry of N_2O_5 and the kinetics of the reaction $N_2O_5 + H_2O \rightarrow 2HNO_3$. *J. Phys. Chem. A* **118**, 11405–11416 (2014).
20. A. Wahner, T. F. Mentel, M. Sohn, J. Stier, Heterogeneous reaction of N_2O_5 on sodium nitrate aerosol. *J. Geophys. Res. Atmos.* **103**, 31103–31112 (1998).
21. J. M. Roberts *et al.*, Laboratory studies of products of N_2O_5 uptake on Cl^- containing substrates. *Geophys. Res. Lett.* **36**, L20808 (2009).
22. W. Behnke, C. George, V. Scheer, C. Zetzsch, Production and decay of $ClNO_2$ from the reaction of gaseous N_2O_5 with NaCl solution: Bulk and aerosol experiments. *J. Geophys. Res. Atmos.* **102**, 3795–3804 (1997).
23. H. D. Osthoff *et al.*, High levels of nitryl chloride in the polluted subtropical marine boundary layer. *Nat. Geosci.* **1**, 324–328 (2008).
24. F. F. Fenter, F. Caloz, M. J. Rossi, Heterogeneous kinetics of N_2O_5 uptake on salt, with a systematic study of the role of surface presentation (for N_2O_5 and HNO_3). *J. Phys. Chem.* **100**, 1008–1019 (1996).
25. S. M. Kane, F. Caloz, M.-T. Leu, Heterogeneous uptake of gaseous N_2O_5 by $(NH_4)_2SO_4$, NH_4HSO_4, and H_2SO_4 aerosols. *J. Phys. Chem. A* **105**, 6465–6470 (2001).
26. G. Robinson, D. Worsnop, J. Jayne, C. Kolb, P. Davidovits, Heterogeneous uptake of $ClONO_2$ and N_2O_5 by sulfuric acid solutions. *J. Geophys. Res. Atmos.* **102**, 3583–3601 (1997).
27. Y. J. Tham *et al.*, Significant concentrations of nitryl chloride sustained in the morning: Investigations of the causes and impacts on ozone production in a polluted region of northern China. *Atmos. Chem. Phys.* **16**, 14959–14977 (2016).
28. C. Yu *et al.*, Heterogeneous N_2O_5 reactions on atmospheric aerosols at four Chinese sites: Improving model representation of uptake parameters. *Atmos. Chem. Phys.* **20**, 4367–4378 (2020).
29. W. Zhou *et al.*, Production of N_2O_5 and $ClNO_2$ in summer in urban Beijing, China. *Atmos. Chem. Phys.* **18**, 11581–11597 (2018).
30. M. Galib, D. T. Limmer, Reactive uptake of N_2O_5 by atmospheric aerosol is dominated by interfacial processes. *Science* **371**, 921–925 (2021).
31. L. Li *et al.*, Formation of HONO from the NH_3-promoted hydrolysis of NO_2 dimers in the atmosphere. *Proc. Natl. Acad. Sci. U.S.A.* **115**, 7236–7241 (2018).

32. S. Ge *et al.*, Abundant NH_3 in China enhances atmospheric HONO production by promoting the heterogeneous reaction of SO_2 with NO_2. *Environ. Sci. Technol.* **53**, 14339–14347 (2019).
33. X. He, J.-J. Wu, Z.-C. Ma, X. Xi, Y.-H. Zhang, NH_3-promoted heterogeneous reaction of SO_2 to sulfate on α-Fe_2O_3 particles with coexistence of NO_2 under different relative humidities. *Atmos. Environ.* **262**, 118622 (2021).
34. S. Wang, X. C. Zeng, H. Li, J. S. Francisco, A possible unaccounted source of atmospheric sulfate formation: Amine-promoted hydrolysis and non-radical oxidation of sulfur dioxide. *Chem. Sci. (Camb.)* **11**, 2093–2102 (2020).
35. S. Wang, H. Li, NO_3·-initiated gas-phase formation of nitrated phenolic compounds in polluted atmosphere. *Environ. Sci. Technol.* **55**, 2899–2907 (2021).
36. J. Almeida *et al.*, Molecular understanding of sulphuric acid-amine particle nucleation in the atmosphere. *Nature* **502**, 359–363 (2013).
37. L. Yao *et al.*, Atmospheric new particle formation from sulfuric acid and amines in a Chinese megacity. *Science* **361**, 278–281 (2018).
38. J. M. Anglada *et al.*, Atmospheric significance of water clusters and ozone-water complexes. *J. Phys. Chem. A* **117**, 10381–10396 (2013).
39. J. Gonzalez *et al.*, The reaction between HO and $(H_2O)n$ ($n = 1$, 3) clusters: Reaction mechanisms and tunneling effects. *Theor. Chem. Acc.* **128**, 579–592 (2011).
40. A. McGuire, "The Boltzmann factor and partition functions" in *Molecular Thermodynamics*, D. A. McQuarrie, J. D. Simon, Ed. (University Science Books, Sausalito, CA, 1999), pp. 105–134.
41. J. VandeVondele *et al.*, Quickstep: Fast and accurate density functional calculations using a mixed Gaussian and plane waves approach. *Comput. Phys. Commun.* **167**, 103–128 (2005).
42. S. Goedecker, M. Teter, J. Hutter, Separable dual-space Gaussian pseudopotentials. *Phys. Rev. B Condens. Matter* **54**, 1703–1710 (1996).
43. C. Hartwigsen, S. Goedecker, J. Hutter, Relativistic separable dual-space Gaussian pseudopotentials from H to Rn. *Phys. Rev. B Condens. Matter Mater. Phys.* **58**, 3641–3662 (1998).
44. S. Grimme, Accurate description of van der Waals complexes by density functional theory including empirical corrections. *J. Comput. Chem.* **25**, 1463–1473 (2004).
45. S. Grimme, Semiempirical GGA-type density functional constructed with a long-range dispersion correction. *J. Comput. Chem.* **27**, 1787–1799 (2006).
46. J. P. Perdew, Y. Wang, Accurate and simple analytic representation of the electron-gas correlation energy. *Phys. Rev. B Condens. Matter* **45**, 13244–13249 (1992).
47. J. P. Perdew, K. Burke, M. Ernzerhof, Generalized gradient approximation made simple. *Phys. Rev. Lett.* **77**, 3865–3868 (1996).
48. C. Lee, W. Yang, R. G. Parr, Development of the Colle-Salvetti correlation-energy formula into a functional of the electron density. *Phys. Rev. B Condens. Matter* **37**, 785–789 (1988).
49. J. Zhong *et al.*, Interaction of the NH_2 radical with the surface of a water droplet. *J. Am. Chem. Soc.* **137**, 12070–12078 (2015).
50. W. G. Hoover, Canonical dynamics: Equilibrium phase-space distributions. *Phys. Rev. A Gen. Phys.* **31**, 1695–1697 (1985).
51. S. Nosé, A unified formulation of the constant temperature molecular dynamics methods. *J. Chem. Phys.* **81**, 511–519 (1984).
52. G. Henkelman, B. P. Uberuaga, H. Jónsson, A climbing image nudged elastic band method for finding saddle points and minimum energy paths. *J. Chem. Phys.* **113**, 9901–9904 (2000).
53. A. Hjorth Larsen *et al.*, The atomic simulation environment—A Python library for working with atoms. *J. Phys. Condens. Matter* **29**, 273002 (2017).